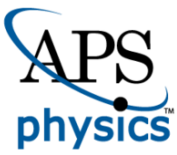

Ultrasound Noncontact Particle Manipulation of Three-dimensional Dynamic User-specified Patterns of Particles in Air

M. Prisbrey and B. Raeymaekers

Phys. Rev. Applied **10**, 034066 — Published 28 September 2018

DOI: 10.1103/PhysRevApplied.10.034066

Ultrasound noncontact particle manipulation of 3D dynamic user-specified patterns of particles in air

M. Prisbrey and B. Raeymaekers*

Department of Mechanical Engineering, University of Utah, Salt Lake City, UT 84112, USA

Abstract

Ultrasound noncontact particle manipulation (NPM) is based on the acoustic radiation force associated with an ultrasound wave field, and enables a myriad of engineering applications with the ability to noninvasively manipulate particles in a fluid medium. We use multiple phased arrays of ultrasound transducers to dynamically move a 3D pattern of particles along a user-specified trajectory following a sequence of affine transformations. We numerically simulate and experimentally validate the NPM method using spherical expanded polystyrene particles in air, and observe good quantitative agreement. The ultrasound NPM method enables dynamic control over the user-specified pattern of particles in three dimensions. Hence, this experimental demonstration shows that ultrasound NPM can be implemented in engineering applications, such as container-less transport and measurement techniques, and manufacturing of engineered materials.

Keywords: ultrasound, noncontact manipulation, phased array

*e-mail: bart.raeymaekers@utah.edu

1. Introduction

Noncontact particle manipulation (NPM) techniques are of critical importance in many engineering applications such as lab-on-chip [1], container-less processing [2], measurement [3], transport [4], chemical analysis [5], and manufacturing engineered materials [6]. Commonly, NPM techniques involve manipulating particles dispersed in a liquid or gas host medium into a user-specified pattern, or along a user-specified trajectory, by means of an electric [7,8], magnetic [9,10], or ultrasound field [11-16] created by a set of transducers. The spatial arrangement and/or operating parameters (amplitude and phase) of the transducer(s) define the external field and, thus, allow control over the locations of the particles within the field. NPM techniques based on magnetic and electric fields restrict particles to be ferromagnetic or electrically conductive, respectively, and/or require high field strengths [7-10], which limits scalability. Ultrasound NPM relies on the convergence of the acoustic radiation force resulting from an ultrasound wave field [17], which creates acoustic "traps" that act as virtual tweezers to hold particles, thus enabling NPM independent of particle properties [18] and shape [19]. Furthermore, ultrasound NPM allows dimensional scalability because the ultrasound wave field experiences low attenuation in low-viscosity fluids (bulk and shear) [20] such as photopolymer resin [6], water [21-23], and air [13-16].

Employing ultrasound NPM in engineering applications requires knowing the relationship between the ultrasound transducer operating parameters, the resulting ultrasound wave field, and the corresponding locations of the particles, which is computed by solving either the forward or inverse ultrasound NPM problem. The forward problem involves computing the location of particles as a function of user-specified ultrasound transducer operating parameters [18,24,25], whereas the inverse problem requires computing the ultrasound transducer operating parameters

needed to place particles in user-specified locations. The inverse problem has been solved to enable static and dynamic ultrasound NPM of a single particle. Greenhall *et al*. [26] derived a theoretical model to determine the location of acoustic traps as a function of the phases of two opposing ultrasound transducers and showed that a particle can be moved along a one-dimensional (1D) line. Marzo *et al.* [14] and Hoshi *et al.* [27] focused acoustic beams to create an acoustic trap located at an arbitrary user-specified position in three-dimensions (3D) to levitate and move expanded polystyrene particles in air. Using four ultrasound transducers arranged in a square, Courtney *et al.* [28] created and moved a 2D "grid" pattern of particles. Furthermore, Greenhall *et al.* [12] derived a 2D solution to the inverse problem and demonstrated the capability to create static 2D user-specified patterns of particles in any 2D domain, with any arbitrary arrangement of ultrasound transducers. Prisbrey *et al*. [11] then expanded this solution to create static 3D user-specified patterns of particles. In this work, we distinguish between static and dynamic ultrasound NPM, respectively, as organizing particles into a single, static user-specified pattern, or moving the pattern of particles along a user-specified trajectory while suspended in the ultrasound field. Although crucial to implementing ultrasound NPM in engineering applications, no experimental demonstration of dynamic ultrasound NPM of multiple particles in 3D exists.

Thus, the objective of this work is to apply the algorithms derived previously by our group for static ultrasound NPM of multiple particles in 3D, and experimentally demonstrate, for the first time, dynamic ultrasound NPM of patterns of multiple particles in 3D. We compute the operating parameters of an arrangement of ultrasound transducers required to create a user-specified pattern of particles that follows a user-specified trajectory. Based on these operating parameters, we numerically simulate and experimentally measure the resulting location of the patterns of particles, and quantify the deviation between user-specified locations, numerical predictions, and

experimental measurements. We implement dynamic ultrasound NPM of multiple particles in 3D using the following three steps. First, we compute the ultrasound wave field as a function of the ultrasound transducer operating parameters (Section 2.1). Then, we apply Gor'kov's acoustic radiation force theory to relate the ultrasound wave field to the locations of acoustic traps, where particles will sit [18] (Section 2.2). Finally, we use the formulation of Greenhall *et al.* [12] to solve the inverse problem and compute the ultrasound transducer operating parameters required to place particles in user-specified locations (Section 2.3). We accomplish dynamic ultrasound NPM by repeating this three-step procedure sequentially, to move the 3D user-specified pattern of particles in discrete increments along a user-specified trajectory.

2. Methods and materials

2.1 Ultrasound wave field simulation

Figure 1 shows a phased array consisting of N_t ultrasound transducers that produce an ultrasound wave field of frequency ω_0. The inset illustrates the spatial parameters to compute the ultrasound wave field in terms of the far-field (complex) pressure **P**, at any discrete domain point $\mathbf{x}_l$ in the domain D (red dots in inset of Fig. 1), which contains a fluid medium of density ρ_0 and sound propagation speed c_0. The pressure field generated by the phased array of ultrasound transducers is

$$\mathbf{P} = \mathbf{B}\mathbf{v}, \tag{1}$$

where $\mathbf{v}^{\mathbf{T}} = (A_1 e^{i\alpha_1}, ..., A_j e^{i\alpha_j}, ..., A_{N_t} e^{i\alpha_{N_t}})$ is a vector containing the operating parameters (amplitude A_j and phase α_j of the ultrasound transducer excitation signal) of each of the N_t ultrasound transducers, with $i = (-1)^{1/2}$. **B** relates the ultrasound transducer operating parameters **v** to the

pressure **P**. Hence, each term p_{lj} of matrix **B** represents the complex pressure at the l^{th} domain point $\mathbf{x}_l$ resulting from the j^{th} ultrasound transducer [29], i.e.,

$$p_{lj} = 2P_0 \frac{J_1(k_0 a \sin\theta_{lj})}{k_0 a \sin\theta_{lj}} \frac{e^{ik_0 r_{lj}}}{r_{lj}}. \tag{2}$$

Here, P_0 is the pressure amplitude (Pa per Vpp square wave excitation signal at a distance from the ultrasound transducer surface) of the j^{th} ultrasound transducer, J_1 is a first order Bessel function of the first kind, $k_0 = 2\pi/\lambda_0$ is the wavenumber and λ_0 is the wavelength of the ultrasound wave field, a is the radius of the ultrasound transducer (piston source), r_{lj} is the 3D Euclidean distance between the l^{th} domain point $\mathbf{x}_l$ and the center point of the j^{th} ultrasound transducer $\mathbf{s}_j$, and θ_{lj} is the angle between $\mathbf{x}_l$ and the normal vector $\mathbf{n}(\mathbf{s}_j)$ that represents the j^{th} transducer surface. In this work, we spatially arrange two phased arrays of N_t transducers opposed to each other to generate a standing ultrasound wave field.

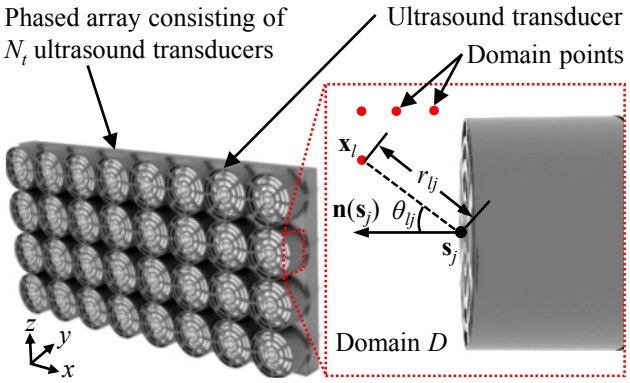

Figure 1. Phased array of N_t ultrasound transducers. The inset illustrates the spatial parameters used to compute the ultrasound wave field at any domain point $\mathbf{x}_l$ (red dots) resulting from the ultrasound transducer centered at $\mathbf{s}_j$ (black dot).

2.2 Acoustic trap locations

Gor'kov's acoustic radiation force theory relates the ultrasound wave field to the locations of the acoustic traps where particles will sit [18]. Acoustic traps are defined as the stable, fixed locations $\mathbf{x}_s$ in D where the acoustic radiation force $\mathbf{f} = -\nabla U$ acting on a spherical particle of radius $r_p << \lambda_0$, density ρ_p, and sound propagation speed c_p is zero and points towards $\mathbf{x}_s$ in the surrounding region. The acoustic radiation potential U, in a fluid with density ρ_0 and sound propagation speed c_0, is locally minimum with respect to the coordinate system (x, y, z) in D at each acoustic trap $\mathbf{x}_s$, and is given as [17,18]

$$U = 2\Phi_1\left(|\,\mathbf{P}\,|^2\right) - 2\Phi_2\left(\left|\frac{\partial \mathbf{P}}{\partial x}\right|^2 + \left|\frac{\partial \mathbf{P}}{\partial y}\right|^2 + \left|\frac{\partial \mathbf{P}}{\partial z}\right|^2\right), \tag{3}$$

with,

$$\Phi_1 = \frac{\pi r_p^3}{3}\left(\frac{1}{c_0^2\rho_0} - \frac{1}{c_p^2\rho_p}\right) \tag{4}$$

$$\Phi_2 = \pi r_p^3\left(\frac{\rho_0 - \rho_p}{\omega_0\rho_0(\rho_0 + 2\rho_p)}\right) \tag{5}$$

2.3 Dynamic manipulation of 3D patterns of particles

To compute the ultrasound transducer operating parameters required to create a 3D user-specified pattern of particles, we minimize the average value of U over all points $\mathbf{x}_l \in \mathrm{X}_i$, where X_i is a matrix that contains the locations of a user-specified pattern of particles. Additionally, we constrain the amplitude of the ultrasound transducers to reflect their finite power output. We then solve a constrained optimization problem using eigendecomposition to compute the optimal operating parameters $\mathbf{v}_i$* of each ultrasound transducer, required to place particles at the user-specified locations X_i [12]. Finally, we sequentially repeat this computation for 3D dynamic NPM of a user-specified pattern of particles along a user-specified trajectory in m - 1 discrete steps. We

determine the user-specified particle locations X_i at each of the m locations of the user-specified trajectory, i.e., $\mathbf{X}_{seq} = X_1,\ldots, X_i,\ldots, X_m$. The transition between each X_i and X_{i+1} is an affine transformation T: $\mathbb{R}^3 \rightarrow \mathbb{R}^3$, i.e., any combination of rotation, scaling, shear mapping, and translation. To move the pattern of particles along the user-specified trajectory, we compute $\mathbf{v}_i^*$ required to drive the particles to the locations specified in each X_i ($1 \leq i \leq m$), thus finding $\mathbf{v}^* = \mathbf{v}_1^*,\ldots, \mathbf{v}_i^*,\ldots, \mathbf{v}_m^*$. Figure 2 illustrates this concept, and shows a pattern of two particles that moves along a user-specified trajectory by sequentially tuning the operating parameters of the arrangement of ultrasound transducers to $\mathbf{v}_1^*$, $\mathbf{v}_2^*$, ...,$\mathbf{v}_m^*$, to move the pattern of particles to the user-specified locations in $X_1, X_2,\ldots, X_m$, respectively.

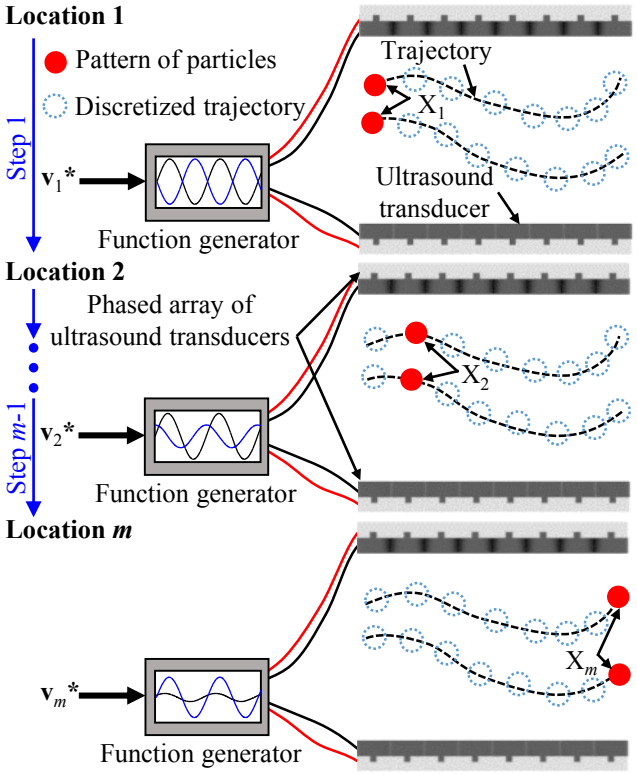

Figure 2. Schematic of a pattern of particles following a user-specified trajectory. Sequentially tuning the operating parameters of the arrangement of ultrasound transducers to $\mathbf{v}_1^*$, $\mathbf{v}_2^*$,...,$\mathbf{v}_m^*$, moves the pattern of particles to the user specified locations defined in X_1, X_2, ...,X_m, respectively.

2.4 Experimental setup

Figure 3 shows a schematic of the experimental setup that consists of two phased arrays of ultrasound transducers, which we use to levitate and move patterns of 2 - 4 mm diameter spherical expanded polystyrene (EPS) (ρ_p = 25 kg/m^3) particles in air. Each phased array comprises a 4×8 arrangement of ultrasound transducers (type Murata MA40S4S) that have a directivity of 80 degrees and a center frequency of 40 kHz, resulting in a wavelength λ_0 = 8.65 mm in air. The angle between the normal vectors $\mathbf{n}_1$ and $\mathbf{n}_2$ of the phased arrays is adjustable by means of two locking hinges, and the minimum distance L is also adjustable.

We employ an Arduino MEGA 2560 equipped with and Ultraino driver shield [30], which drives each ultrasound transducer using an independently controlled pulse width modulated PWM signal with frequency 40 kHz and amplitude 5 Vpp. Figure 3 does not depict the wires that carry the 40 kHz signal from the driver shield to each ultrasound transducer (for clarity), but instead shows them as blue dashed arrows. Altering the PWM duty cycle and adding a delay to the signal (using the Ultraino software [30]), respectively, allows independently adjusting the amplitude and phase of each ultrasound transducer.

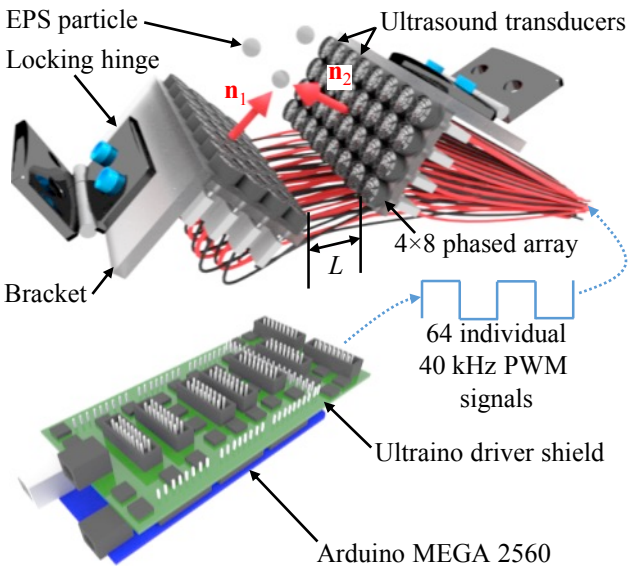

Figure 3. Schematic of the experimental setup with two phased arrays that each comprise an arrangement of 4×8 ultrasound transducers, driven by a 40 kHz pulse-width modulation signal using an Arduino MEGA 2560.

3. Results and discussion

Figures 4-8 show 3D dynamic ultrasound NPM of several user-specified patterns of EPS particles along a user-specified trajectory. We demonstrate dynamic control over a pattern of particles in a single plane by performing a translation (Fig. 4), rotation (Fig. 5), scaling and shear mapping (Fig. 6), and combined translation and rotation (Fig. 7) of the user-specified pattern of particles. We also show 3D ultrasound NPM in multiple planes by performing a translation and rotation (Fig. 8). These experiments and simulations demonstrate simultaneous and individual control over subsets and/or the entire pattern of particles.

Figures 4(a)-7(a) depict the user-specified pattern of particles at its initial location (X_1). The inset image shows a side view of the user-specified pattern of particles (red dots), the simulated pattern of particles (blue dots) that we determine by computing the acoustic radiation force based on $\mathbf{v}_i$* after solving the constrained optimization problem (see Section 2.3), and a photograph of the experimentally obtained pattern of particles (gray), at several locations X_i along the user-specified trajectory of the pattern of particles. Figures 4(b)-7(b) show the pattern error E_{pat}, which we compute as the mean distance between the centroids of the user-specified and the simulated and experimentally obtained particle locations, respectively, normalized by the wavelength of the standing ultrasound wave field λ_0 = 8.65 mm, for each pattern location along the user-specified trajectory. The upper and lower limits of the error bars represent the maximum and minimum pattern error at each location, respectively.

Figure 4 illustrates the combination of multiple phased arrays, and shows a "V-shape" configuration of two phased arrays with a 70-degree angle between vectors $\mathbf{n}_1$ and $\mathbf{n}_2$ and $L = 2.3\lambda_0$, which ensures that all particles remain in the far-field. We define a user-specified pattern of three particles located at the corners of a triangle with base $3.2\lambda_0$ and height $1.2\lambda_0$, which contrasts existing ultrasound NPM methods for creating static 3D user-specified patterns of particles that

are limited to rectangular grid or line patterns [11,12]. The pattern of particles follows a trajectory that consists of a sequence of translations from its initial location (X_1, magenta) over a distance λ_0 in the positive z-direction (ten steps, X_{11}, green), then a distance $0.35\lambda_0$, in the positive x-direction (three steps, X_{14}, yellow), and a distance $0.7\lambda_0$ in the negative x-direction (five steps, X_{19}, cyan).

Figure 5 shows an "opposing" configuration of two phased arrays oriented with an angle of 180 degrees between vectors $\mathbf{n}_1$ and $\mathbf{n}_2$ (co-linear) and $L = 8\lambda_0$, to demonstrate manipulating particles in a setup with negligible wave propagation in the z-direction to counteract gravity. We define a user-specified pattern of four particles spaced λ_0 apart along a line, and rotate the pattern of particles about the z-axis over 50 degrees in ten steps. Figure 5(a) shows the pattern in its initial location (X_1, magenta), after rotating 20 degrees (four steps, X_5, green), and after rotating 50 degrees (ten steps, X_{11}, cyan). This trajectory requires that in each step, each particle simultaneously moves over a different distance and in a different direction, in contrast with the trajectory of Fig. 4, where each particle (of the pattern) undergoes an identical translation in each step along the trajectory. Thus, this method enables control of the location of the entire pattern of particles, or a subset thereof.

Figure 6 shows the same configuration of phased arrays as Fig. 5, but we define a user-specified pattern of four particles at the corners of a $\lambda_0 \times 2.75\lambda_0$ rectangle. We scale the pattern of particles in the y-direction by a factor 1.7, i.e., two particles move in the positive and negative y-direction, respectively. We then shear map the rectangle in the x-direction in the xy-plane. Figure 6(a) shows the pattern in its initial location (X_1, magenta), after scaling (four steps, X_5, green), and after shear mapping (seven steps, X_{12}, cyan). The trajectory shown in Fig. 6 requires that in each step, a group of particles simultaneously moves in a different direction, in contrast with the trajectory of Figs. 4 and 5, where either each particle undergoes an identical translation in each

step along the trajectory, or each particle is individually controlled. Thus, this method allows controlling subgroups of particles within the pattern of particles.

Figure 7 shows the same configuration of phased arrays as Figs. 5 and 6, but we rearrange the phased arrays to be at the top and bottom (*xy*-plane rather than *yz*-plane in Figs. 5 and 6). We define a user-specified pattern of three particles spaced $3\lambda_0/2$ apart along a line, and rotate the pattern of particles over 70 degrees about the center point of the line pattern (middle particle, about the *x*-axis), and simultaneously the center point translates $3.25\lambda_0$ in the *y*-direction. Figure 7(a) shows the pattern in its initial location (X_1, magenta), after rotating 37 degrees and translating $1.75\lambda_0$ (eight steps, X_9, green), and after reaching its final location (six steps, X_{15}, cyan). The trajectory shown in Fig. 7 requires that in each step, the pattern of particles simultaneously performs a translation and rotation, which contrasts with the trajectories of Figs. 4, 5, and 6.

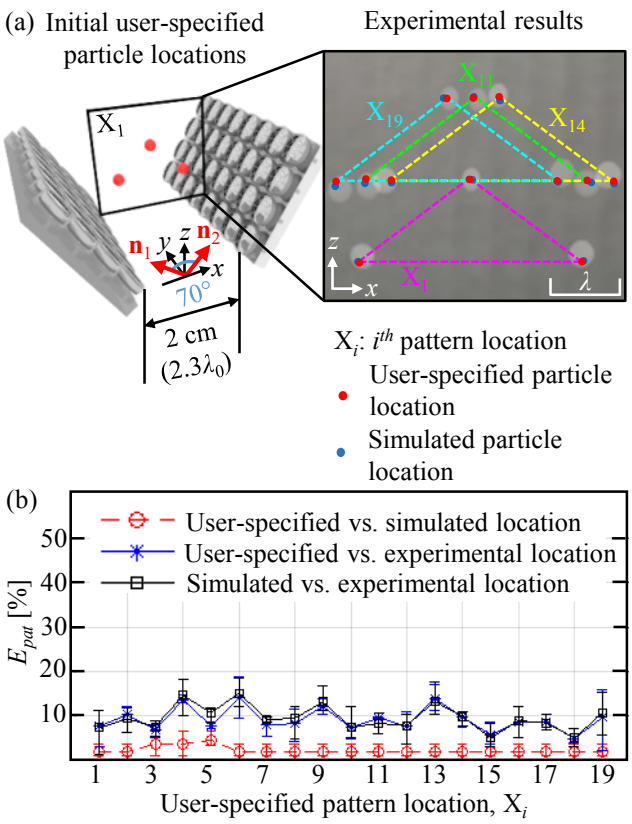

Figure 4. (a) User-specified (red), simulated (blue), and experimentally obtained pattern of particles (grey), shown at locations 1, 11, and 19. (b) Pattern error between user-specified, simulated, and experimentally obtained particle locations at each pattern location.

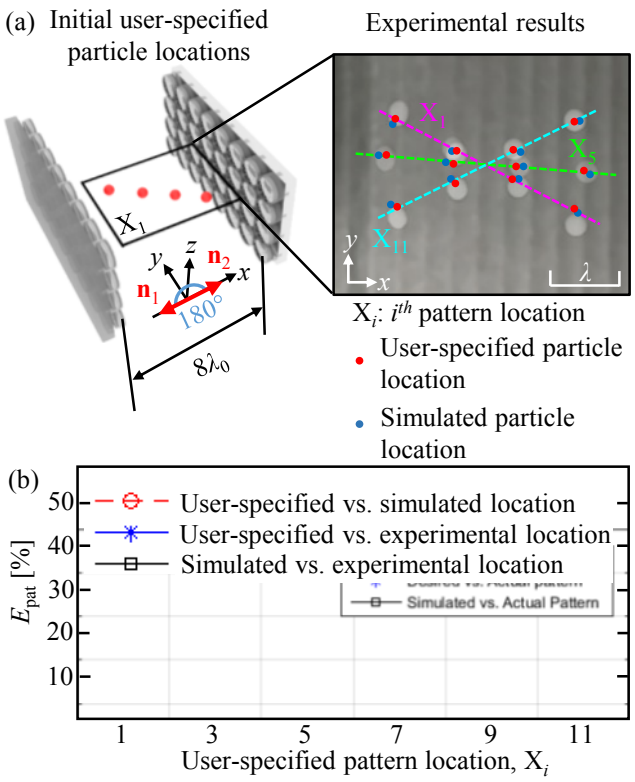

Figure 5. (a) User-specified (red), simulated (blue), and experimentally obtained pattern of particles (grey), shown at locations 1, 5, and 11. (b) Pattern error between user-specified, simulated, and experimentally obtained particle locations at each pattern location.

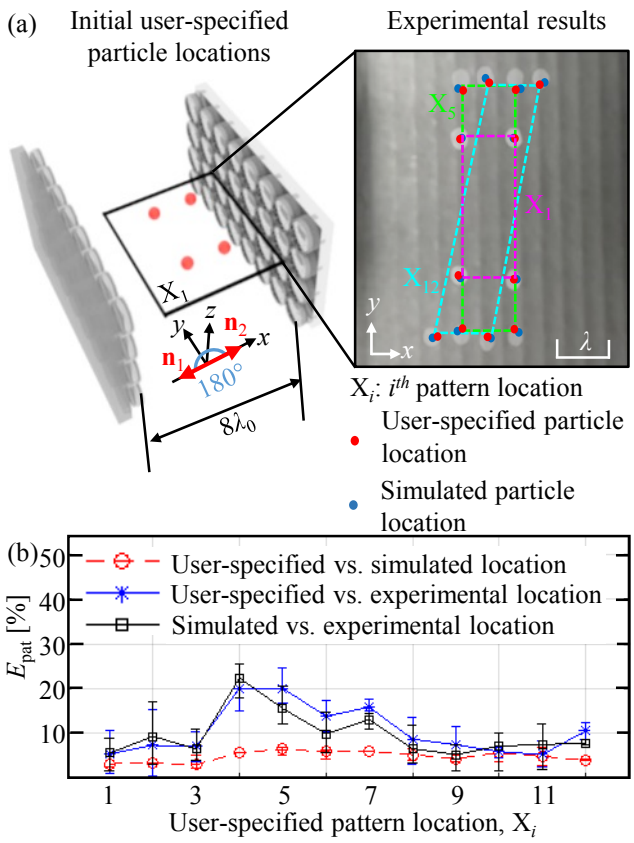

Figure 6. (a) User-specified (red), simulated (blue), and experimentally obtained pattern of particles (grey), shown at location 1, 5, and 12. (b) Pattern error between user-specified, simulated, and experimentally obtained particle locations at each pattern location.

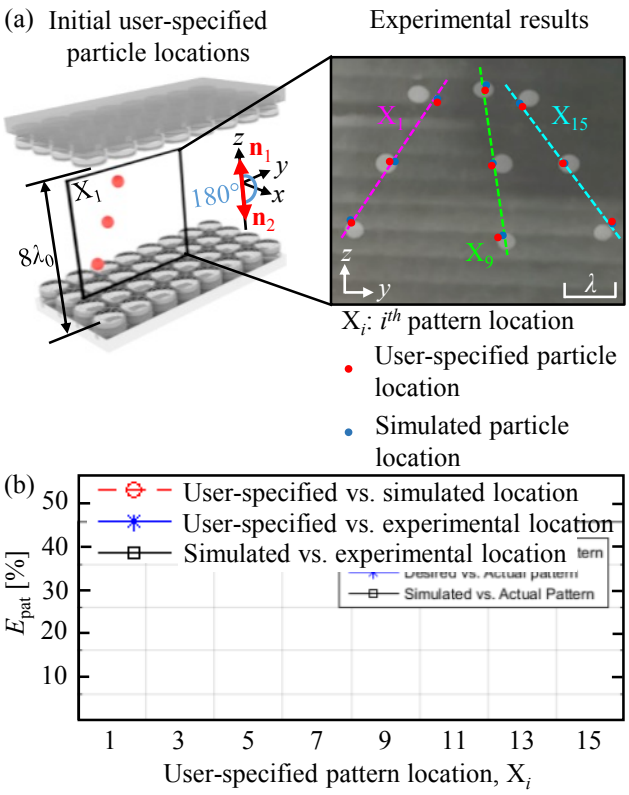

Figure 7. (a) User-specified (red), simulated (blue), and experimentally obtained pattern of particles (grey), shown at location 1, 9, and 15. (b) Pattern error between user-specified, simulated, and experimentally obtained particle locations at each pattern location.

We compute a maximum pattern error of 31.3% for all experiments documented in Figs. 4-7, which we observe in Fig. 5(b) between the simulated and experimentally obtained particle locations. However, the pattern error remains below 20.0% in 86% of all cases, indicating good quantitative agreement between user-specified, simulated, and experimental particle locations. We also note that these experiments are repeatable within the specified range of operating conditions, resulting in similar pattern errors each repetition. Differences between the user-specified, simulated, and experimental particle locations are due to non-perfectly spherical EPS particles, and primary and secondary ultrasound wave field scattering off nearby surfaces and neighboring particles, respectively, which is not accounted for in the far-field piston source method used in the

numerical model. Additionally, imperfections in manufacturing the experimental setup (*e.g.* misaligned transducers) and limited resolution of amplitude and phase adjustments in the Ultraino software and Arduino, contribute to the pattern error. Figures 4-7 show dynamic patterns of particles in a single plane, which only requires affine transformations in that plane. However, because we control the x, y, and z positions of each particle in the patterns, assembling these patterns of particles requires accounting for the acoustic radiation force in the x, y, and z-directions, which requires computing a 3D ultrasound wave field. Hence, the small pattern error of the experimental results demonstrates the capability of this method to enable 3D dynamic ultrasound NPM of a user-specified pattern of particles along a user-specified trajectory.

We also present 3D patterns of particles simultaneously undergoing affine transformations in multiple xy-planes, using the same configuration of phased arrays as shown in Fig. 7. Figure 8(a) shows a user-specified pattern of eight particles at the corners of a $3.5\lambda_0 \times 3.5\lambda_0 \times \lambda_0$ cuboid. We translate the pattern of particles in the y-direction over $1.85\lambda_0$ in the y-direction in eight steps. Figure 8(b) shows a pattern of three particles spaced $\lambda_0/2$ apart along a line, parallel to the z-axis. We rotate the pattern of particles about the z-axis in a circle of radius $1.5\lambda_0$ in 37 steps over 360 degrees. Figures 8(a) and (b) show a schematic of the experimental setup on the left, with the intended trajectory indicated by a blue arrow. The experimental results are shown on the right for different locations X_i. We qualitatively observe good agreement between the user-specified particle locations and the intended trajectory of the pattern. The trajectories shown in Figs. 4-7 required moving a 2D pattern of particles in a single plane. In contrast, Fig. 8 demonstrates that the algorithm and method presented in this work allows moving a 3D user-specified pattern of particles along a user-specified trajectory.

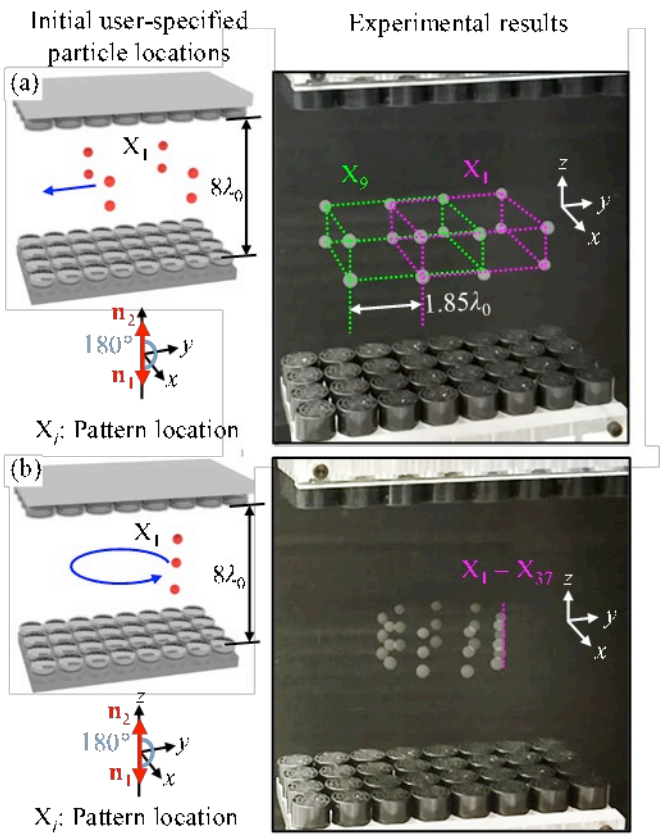

Figure 8. Experimental results moving a 3D pattern of particles along a user-specified trajectory, for (a) a cuboid translating in the *y*-direction and (b) a column of particles rotating around a vertical axis.

We levitate EPS particles in air to experimentally demonstrate and visualize that the ultrasound NPM algorithm allows manipulating patterns of particles along a user-specified trajectory. However, we emphasize that the algorithm translates to systems of different size and shape, with different fluids and particles. Hence, the algorithms apply to e.g. using ultrasound NPM as a processing method for engineered materials that derive their function from a pattern of particles embedded in a matrix material. Additionally, because it enables prescribing a user-specified trajectory for each particle in a pattern of particles, the algorithm and method is suitable for lab-on-chip and container-less transport, including drug delivery applications.

Dynamic ultrasound NPM of a 3D user-specified pattern of particles along a user-specified trajectory discretized in m locations requires changing the acoustic traps of the ultrasound standing wave field from X_i to X_{i+1} (see Section 2.3). The maximum achievable translation distance from X_i to X_{i+1} depends on the ultrasound transducer arrangement, the direction of movement, and the strength of acoustic trap. For the transducer arrangement of Fig. 8, and for a single trap strength, Marzo *et el.* [14] experimentally determined the maximum achievable translation distance in a single step in the x, y, and z-directions to be $0.84\lambda_0$, $0.82\lambda_0$, and $0.25\lambda_0$, respectively. The corresponding maximum speed achieved for particle movement in this setup is $33.5\lambda_0$ per second, $33.5\lambda_0$ per second, and $0.59\lambda_0$ per second, in the x, y, and z-directions, respectively, and is limited by the electronics that drive the system [14]. The dynamic behavior of EPS particles in air while in transition from X_i to X_{i+1} has not been fully characterized, and requires considering the acoustic radiation force, and Stokes and Oseen drag forces [22, 35]. We note that although we did not observe this behavior in our experiments, it is theoretically possible for a particle to experience large amplitude vibrations around an acoustic trap, when the acoustic radiation force becomes much larger than the drag force imposed on the particle by the surrounding fluid [22], and the system is underdamped.

We quantify the success rate of moving an EPS particle over a distance Δz from its user-specified particle location in X_i to that in X_{i+1}, as a function of the acoustic trap strength S in X_{i+1}. S is defined as the amplitude of the complex pressure magnitude $|\mathbf{P}|$ in the region $\pm\lambda_0/2$ surrounding the acoustic trap in the z-direction, which we determine by simulating the ultrasound field (see Section 2.1). We define Δz opposite to gravity because this is the case that requires the largest potential energy increase to the particle. Figure 9 shows the rate of successfully translating a particle, R_s, as a function of the normalized translation distance $\Delta z/\Delta z_{max}$ and trap strength S/S_{min}.

S_{min} is the trap strength that results in an acoustic radiation force that is equal to the gravitational force acting on a particle in the positive z-direction. Δz_{max} is the theoretical maximum single step translation distance. We determine the maximum single step translation distance by computing the distance between the location of the acoustic trap in X_{i+1} and the nearest local pressure maximum in the direction of the acoustic trap location in X_i, i.e., $\Delta z_{max} = \lambda_0/4$ for this arrangement of phased arrays. We calculate R_s as the number of successful translations from the particle location in X_i to the particle location in X_{i+1} out of ten attempts. For each of the ten attempts we choose a random spherical EPS particle 2-4 mm in diameter. The inset of Fig. 9 shows a phased array configuration with co-linear normal vectors, $\mathbf{n}_1$ and $\mathbf{n}_2$, aligned with the z-axis (identical to Fig. 7). From Fig. 9, we observe that a trap strength at least seven times stronger than the minimum trap strength required to levitate a spherical particle yields R_s = 100% of translating that particle over $\Delta z_{\max}$. When R_s is less than 100%, we observe that the particles are ejected from the ultrasound field or become fixed in an acoustic trap that is not at the user-specified particle location in X_{i+1}. At S/S_{min} = 6 and $\Delta z/\Delta z_{max}$ = 0.8 we counterintuitively observe that R_s is smaller than R_s at a greater translation distance and smaller trap strength, specifically at S/S_{min} = 5 and $\Delta z/\Delta z_{max}$ = 0.9. Similar to Marzo *et al.* [16] we speculate that this counter-intuitive result is due to the randomly chosen EPS particles at S/S_{min} = 6 and $\Delta z/\Delta z_{max}$ = 0.8 being irregularly shaped, which causes uneven scattering that becomes pronounced during the movement process between X_i and X_{i+1} [22]. We hypothesize that the uneven scattering increases the possibility for the particle to be perturbed away from X_{i+1}.

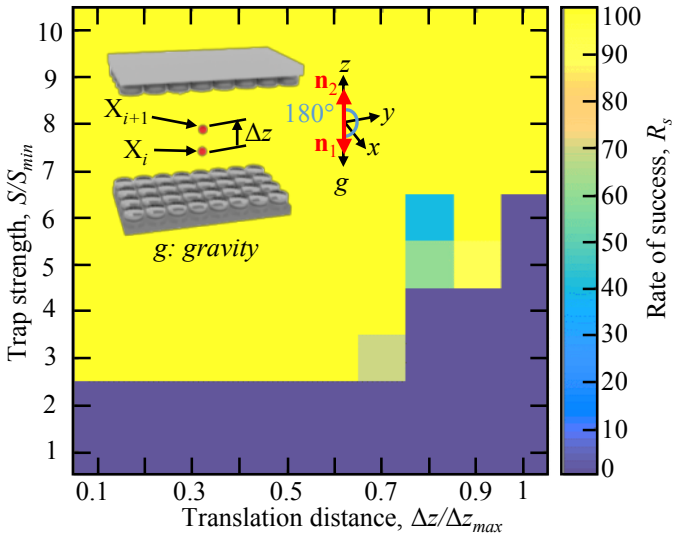

Figure 9. Rate of successfully translating a particle R_s, as a function of the normalized translation distance $\Delta z/\Delta z_{max}$ and trap strength S/S_{min}.

Acoustic traps that are not located at user-specified particle locations are an inevitable result of interference between the pressure waves generated by the ultrasound transducers. In Figs. 4-8, we specify patterns of particles that yield acoustic traps with a large enough strength to levitate a spherical particle in every specified location. However, it is possible to specify a pattern of particles for which not all acoustics traps have a large enough strength to levitate a particle. We also specify affine transformations in which all the acoustic traps created at user-specified locations in X_{i+1} have a trap strength large enough to allow translation from X_i. It is possible to specify affine transformations that will not yield acoustic traps with a large enough strength to enable translation to all user-specified locations in X_{i+1}. Additionally, it is possible to specify a pattern of particles that will not yield acoustic traps in all specified locations, *e.g.* acoustic traps that are located a sub-half-wavelength distance from each other. The relationship between the

range of all possible patterns, transformations of patterns, frequency and arrangement of the ultrasound transducers remains an open problem.

Prior to this work, ultrasound NPM methods show static and dynamic manipulation of a single particle in 1D [26] and 3D [14,27], by computing the ultrasound transducer operating parameters required to generate an acoustic trap in a single user-specified location in the ultrasound wave field for a single location of the particle or a sequence of locations. Other methods enable static and dynamic manipulation of multiple particles in 2D [12,28,31-24] by computing the ultrasound transducer operating parameters required to create acoustic traps in multiple user-specified locations. These methods approximate the wave field created by the ultrasound transducers, and only account for ultrasound field variations in 2D, thus limiting particle manipulation in the third dimension. One method enables static manipulation of multiple particles in 3D [11] by computing the required ultrasound transducer operating parameters to generate acoustic traps in multiple user-specified locations and accounts for ultrasound field variations in 3D, allowing for manipulation in 3D, but only does so for stationary patterns. In contrast, this work demonstrates an ultrasound NPM method that computes the ultrasound transducer operating parameters required to generate acoustic traps in multiple user-specified locations in 3D for a sequence of patterns, which allows creating dynamic user-specified patterns of particles in 3D.

4. Conclusion

We have simulated and experimentally demonstrated a noncontact particle manipulation method for creating dynamic 3D user-specified patterns of particles using a standing ultrasound wave field. This contrasts existing works that are limited to dynamic manipulation of single particles and to creating static 2D and 3D patterns of particles. We show that the solution of the

inverse ultrasound NPM problem, using the formulation of Greenhall *et al.*, enables accurate affine transformations of patterns of particles in 3D, as indicated by good quantitative agreement between user-specified, simulated, and experimentally obtained patterns of particles. We also experimentally demonstrate that an acoustic trap strength of seven times the trap strength required to levitate a particle is needed to successfully translate that particle over a single step translation distance of $\lambda_0/4$ with a 100% rate of success. This knowledge enables using ultrasound as a noncontact particle manipulation technique in several engineering and research applications, including lab-on-chip and container-less processing and transport.

Acknowledgments

This research was supported by the Army Research Office under contract no. W911NF-16-1-0457.

References

[1] Ding, X., Lin, S., Kiraly, B., Yue, H., Li, S., Chiang, I., Shi, J., Benkovic, S., & Huang, T. On-chip manipulation of single microparticles, cells, and organisms using surface acoustic waves. Proc. Natl. Acad. Sci. U. S. A. **109**, 11105 (2012).

[2] Rey, C. A., Merkley, D. R., Hammarlund, G. R. & Danley, T. J. Acoustic levitation at high temperatures in the microgravity of space. J. Acoust. Soc. Am. **82,** S106 (1987).

[3] Trinh, E. H. & Ohsaka, K. Measurement of density, sound velocity, surface tension, and viscosity of freely suspended supercooled liquids. Int. J. Thermophys. **16**, 545 (1995).

[4] Whymark, R. R. Acoustic field positioning for containerless processing. Ultrasonics **13**, 251 (1975).

[5] Santesson, S. & Nilsson, S. Airborne chemistry: acoustic levitation in chemical analysis. Anal. Bioanal. Chem. **378**, 1704 (2004).

[6] Greenhall, J. & Raeymaekers, B. 3D Printing Macroscale Engineered Materials Using Ultrasound Directed Self-Assembly and Stereolithography. Adv. Mater. Technol. **2**, 1700122 (2017).

]7] Kamat, P. V., Thomas, K. G., Barazzouk, S., Girishkumar, G., Vinodgopal, K. & Miesel, D. Self-assembled linear bundles of single wall carbon nanotubes and their alignment and deposition as a film in a dc field. J. Am. Chem. Soc. **126**, 10757 (2004).

[8] Yang, Y., Chen, Z., Song, X., Zhang, Z., Zhang, J., Shung, K. K., Zhou, Q. & Chen, Y. Biomimetic Anisotropic Reinforcement Architectures by Electrically Assisted Nanocomposite 3D Printing. Adv. Mater. **29**, 1605750(2017).

[9] Promislow, J. H. E. & Gast, A. P. Magnetorheological Fluid Structure in a Pulsed Magnetic Field. Langmuir **12,** 4095 (1996).

[10]. Martin, J. J., Fiore, B. E. & Erb, R. M. Designing bioinspired composite reinforcement architectures via 3D magnetic printing. Nat. Commun. **6,** 9641 (2015).
[11]. Prisbrey, M., Greenhall, J., Guevara Vasquez, F. & Raeymaekers, B. Ultrasound directed self-assembly of three-dimensional user-specified patterns of particles in a fluid medium. J. Appl. Phys. **121**, 014302 (2017).
[12] Greenhall, J., Guevara Vasquez, F. & Raeymaekers, B. Ultrasound directed self-assembly of user-specified patterns of nanoparticles dispersed in a fluid medium. Appl. Phys. Lett. **108**, 103103 (2016).
[13] Ochiai, Y., Hoshi, T. & Rekimoto, J. Three-Dimensional Mid-Air Acoustic Manipulation by Ultrasonic Phased Arrays. PLOS ONE **9**, e102525 (2014).
[14] Marzo, A., Seah, S. A., Drinkwater, B. W., Sahoo, D. R., Long, B. & Subramanian, S. Holographic acoustic elements for manipulation of levitated objects. Nat. Commun. **6**, 9661 (2015).
[15] Foresti, D., Nabavi, M., Klingauf, M., Ferrari, A. & Poulikakos, D. Acoustophoretic contactless transport and handling of matter in air. Proc. Natl. Acad. Sci. **110**, 12549 (2013).
[16] Marzo, A., Barnes, A. & Drinkwater, B. W. TinyLev: A multi-emitter single-axis acoustic levitator. Rev. Sci. Instrum. **88**, 085105 (2017).
[17] Bruus, H. Acoustofluidics 7: The acoustic radiation force on small particles. Lab. Chip **12**, 1014 (2012).
[18] Gor'kov, L. P. On the Forces Acting on a Small Particle in an Acoustical Field in an Ideal Fluid. Sov. Phys. Dokl. **6**, 773 (1962).
[19] Collino, R. R., Ray, T. R., Fleming, R. C., Sasaki, C. H., Haj-Hariri, H. & Begley, M. R. Acoustic field controlled patterning and assembly of anisotropic particles. Extreme Mech. Lett. **5**, 37 (2015).
[20] L.E. Kinsler, Frey, A. R., Coppens, A. B. & Sanders, J. V. Fundamentals of Acoustics. (John Wiley, New York, 2000).
[21] Courtney, C. R. P. et al. Dexterous manipulation of microparticles using Bessel-function acoustic pressure fields. Appl. Phys. Lett. **102**, 123508 (2013).
[22] Greenhall, J., Guevara Vasquez, F. & Raeymaekers, B. Dynamic behavior of microscale particles controlled by standing bulk acoustic waves. Appl. Phys. Lett. **105**, 144105 (2014).
[23] Raeymaekers, B., Pantea, C. & Sinha, D. N. Manipulation of diamond nanoparticles using bulk acoustic waves. J. Appl. Phys. **109**, 014317 (2011).
[24] Barmatz, M. & Collas, P. Acoustic radiation potential on a sphere in plane, cylindrical, and spherical standing wave fields. J. Acoust. Soc. Am. **77**, 928 (1985).
[25] Chen, X. & Apfel, R. E. Radiation force on a spherical object in an axisymmetric wave field and its application to the calibration of high-frequency transducers. J. Acoust. Soc. Am. **99**, 713 (1996).
[26] Greenhall, J., Guevara Vasquez, F. & Raeymaekers, B. Continuous and unconstrained manipulation of micro-particles using phase-control of bulk acoustic waves. Appl. Phys. Lett. **103**, 074103 (2013).
[27] Hoshi, T., Ochiai, Y. & Rekimoto, J. Three-dimensional noncontact manipulation by opposite ultrasonic phased arrays. Jpn. J. Appl. Phys. **53**, 07KE07 (2014).
[28] Courtney, C. R. P., Ong, C.-K., Drinkwater, B. W., Bernassau, A. L., Wilcox, P. D. & Cumming, D. R. S. Manipulation of particles in two dimensions using phase controllable ultrasonic standing waves. Proc. R. Soc. A. **468**, 337 (2011).
[29] Cheeke, D. Fundamentals and Applications of Ultrasonic Waves. (CRC Press LLC, 2002).
[30] Marzo, A., Corkett, T., & Drinkwater, B. W. Ultraino: an Open Phased-Array System for Narrowband Airborne Ultrasound Transmission. IEEE Trans. Ultrason. Ferroelectr. Freq. Control. **65,** 102 (2017).

[31] Courtney, C. R. P., Demore, C. E. M., Wu, H., Grinenko, A., Wilcox, P. D., Cochran, S. & Drinkwater, B. W. Independent trapping and manipulation of microparticles using dexterous acoustic tweezers. Appl. Phys. Lett. **104**, 154103 (2014).
[32] Bernassau, A. L., Courtney, C. R. P., Beeley, J., Drinkwater, B. W. & Cumming, D. R. S. Interactive manipulation of microparticles in an octagonal sonotweezer. Appl. Phys. Lett. **102**, 164101 (2013).
[33] Bernassau, A. & Cumming, D. R. S. Acoustic Tweezing at the Nodes or Antinodes of a Heptagonal Multi Piezoelectric Transducer Cell. 1537 (2011).
[34] Grinenko, A., Wilcox, P. D., Courtney, C. R. P. & Drinkwater, B. W. Proof of principle study of ultrasonic particle manipulation by a circular array device. Proc. R. Soc. A. **468**, 3571 (2012).
[35] Westervelt, P.J., The theory of steady forces caused by sound waves. J. Acoust. Soc. Am. **23** 312 (1951)